Developmental Biology 379 (2013) 258–269

Contents lists available at SciVerse ScienceDirect

Developmental Biology

journal homepage: www.elsevier.com/locate/developmentalbiology

Mathematical model of a gene regulatory network reconciles effects of genetic perturbations on hematopoietic stem cell emergence

Jatin Narula [a,1], C.J. Williams [a,1], Abhinav Tiwari [a,1], Jonathon Marks-Bluth [b], John E. Pimanda [b,*], Oleg A. Igoshin [a,**]

[a] Department of Bioengineering, Rice University, Houston, TX, USA
[b] Lowy Cancer Research Centre and the Prince of Wales Clinical School, University of New South Wales, Sydney, NSW 2052, Australia

ARTICLE INFO

Article history:
Received 18 December 2012
Received in revised form
6 April 2013
Accepted 17 April 2013
Available online 23 April 2013

Keywords:
Hematopoietic stem cells
Bistability
Bmp signaling
Notch signaling
Runx1

ABSTRACT

Interlinked gene regulatory networks (GRNs) are vital for the spatial and temporal control of gene expression during development. The hematopoietic transcription factors (TFs) Scl, Gata2 and Fli1 form one such densely connected GRN which acts as a master regulator of embryonic hematopoiesis. This triad has been shown to direct the specification of the hemogenic endothelium and emergence of hematopoietic stem cells (HSCs) in response to Notch1 and Bmp4–Smad signaling. Here we employ previously published data to construct a mathematical model of this GRN network and use this model to systematically investigate the network dynamical properties. Our model uses a statistical-thermodynamic framework to describe the combinatorial regulation of gene expression and reconciles, mechanistically, several previously published but unexplained results from different genetic perturbation experiments. In particular, our results demonstrate how the interactions of Runx1, an essential hematopoietic TF, with components of the Bmp4 signaling pathway allow it to affect triad activation and acts as a key regulator of HSC emergence. We also explain why heterozygous deletion of this essential TF, Runx1, speeds up the network dynamics leading to accelerated HSC emergence. Taken together our results demonstrate that the triad, a master-level controller of definitive hematopoiesis, is an irreversible bistable switch whose dynamical properties are modulated by Runx1 and components of the Bmp4 signaling pathway.

© 2013 Elsevier Inc. All rights reserved.

Introduction

Hematopoietic stem cells (HSCs) are a rare population of cells with self-renewal potential to divide and contribute cells to all blood lineages throughout the life of an organism. The ontogeny of HSCs has been carefully studied in terms of anatomical locations and stages of cellular progression (Medvinsky et al., 2011; Orkin and Zon, 2008). Studies using mouse, zebrafish and embryonic stem cells have demonstrated that blood progenitor cells (with limited self-renewal ability) are formed early during embryogenesis, initially in the yolk sac and then in the embryo (Medvinsky et al., 2011). This is followed by the emergence of definitive HSCs (with long-term self-renewal potential) initially in the aorta-gonads-mesonephros region of both mice and humans (Medvinsky et al., 2011). Furthermore, it has been shown that a specialized part of the blood vessel network termed the 'hemogenic endothelium' undergoes an endothelial-to-hematopoietic transition (EHT) to form blood stem/progenitor cells (Bertrand et al., 2010; Boisset et al., 2010; Eilken et al., 2009; Lancrin et al., 2009; Zovein et al., 2008). Understanding the molecular mechanisms that drive HSC and blood formation in the developing embryo will be crucial in designing novel regenerative medicine protocols.

Tight spatial and temporal control of gene expression is vital for the proper development of an organism (Davidson, 2006). Gene expression programs are coordinately regulated by the combinatorial binding of tissue-specific transcription factors (TFs) and external cues that are communicated to cells via signaling pathways. Several TFs regulating key stages of blood cell development have been identified (Marks-Bluth and Pimanda, 2012). Scl, Gata2 and Fli1 act early during development to specify the hemogenic endothelium and are necessary for HSC emergence (Hart et al., 2000; Ling et al., 2004; Schlaeger et al., 2005; Shivdasani et al., 1995; Tsai et al., 1994). On the other hand, Runx1 is required in the hemogenic endothelium for the EHT but not subsequently (Chen et al., 2009; Li et al., 2006; Liakhovitskaia et al., 2009). TF activities and signaling pathways are integrated by *cis*-regulatory modules such as promoters and enhancers which have been characterized for numerous TFs involved in HSC emergence (Pimanda and Gottgens, 2010). Enhancers for *Gata2, Fli1* and *Scl* are bound by

* Corresponding author.
** Corresponding author.
E-mail addresses: jpimanda@unsw.edu.au (J.E. Pimanda), igoshin@rice.edu (O.A. Igoshin).
[1] These authors contributed to the work equally.

0012-1606/$ - see front matter © 2013 Elsevier Inc. All rights reserved.
http://dx.doi.org/10.1016/j.ydbio.2013.04.016

themselves and each other to form a fully connected triad (Pimanda et al., 2007b), and the HSC enhancer for *Runx1* is bound by all three triad proteins (Nottingham et al., 2007).

Two signaling pathways, Bmp and Notch, are required for HSC and progenitor development (Durand et al., 2007; Kaimakis et al., 2013; Kumano et al., 2003; Marks-Bluth and Pimanda, 2012). The Notch1 intracellular mediator binds at the *Gata2* locus, whereas Bmp-induced signaling mediator, Smad1, binds at the *Runx1* promoter and at the *Gata2* and *Fli1* enhancers (Fig. 1A; (Oren et al., 2005; Pimanda et al., 2007a; Robert-Moreno et al., 2005)). Smad6, an inhibitory Smad, participates in the Bmp4-signaling pathway by hindering Smad1 activation and targeting it for proteolytic degradation (Knezevic et al., 2011). The *Smad6* enhancer is bound by the triad proteins, Smad1 and Runx1, and a negative feedback loop from Smad6 regulates Runx1 by promoting its proteosomal degradation (Knezevic et al., 2011). Runx1 binding at the *Smad6* enhancer is mediated by triad TFs, thus triad activation temporally balances Runx1 activity by up-regulating both Runx1 and its negative regulator Smad6 (Knezevic et al., 2011). Altogether these interactions form a gene regulatory network (GRN) that controls hematopoietic stem and progenitor cell emergence in the developing embryo (Fig. 1B). Multiple feed-forward and feedback loops present in the GRN (Fig. 1A) lead to complex dynamical properties that allow tight control over the network's response to external and internal cues. Understanding these complex emergent properties with purely experimental approaches is challenging; mathematical modeling of networks can serve as an important complementary approach. Models can combine qualitative and quantitative information about network architecture and parameters, and thereby serve as an integrative platform for understanding the results of various genetic perturbations and for making novel predictions.

In this study, we build a mathematical model of the GRN shown in Fig. 1B based on previously published details of *cis*-regulatory modules, TF-binding and protein–protein interactions. The model integrates Runx1 regulation as well as Bmp4 and Notch1 signaling with the Scl–Gata2–Fli1 triad module. Using this model we elucidate the role of Runx1 in the network. Dynamical properties of the network predicted by the model are in good agreement with in vitro and in vivo experimental observations. Moreover, *in silico* perturbations of Runx1, Notch1 and Bmp4 in the simulations closely match the observations in knockout and over-expression phenotypes. Importantly, our model provides mechanistic insight into the early emergence of blood progenitors observed in *Runx1* haploid embryos. Taken together these results suggest that the GRN analyzed here can act as a master-level switch in the signal pathway controlling definitive hematopoiesis.

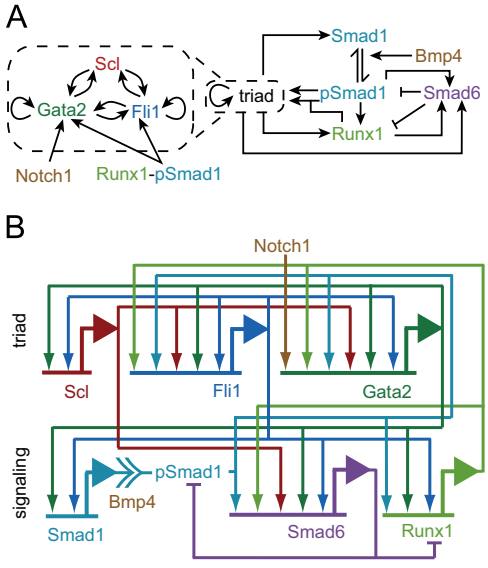

Fig. 1. GRN responsible for regulating HSC specification. (A) The GRN responsible for regulating HSC cell specification contains TFs Scl, Gata2, and Fli1 that are connected via multiple positive feedback loops (dashed box). This triad is regulated directly via Notch1 and indirectly via Bmp4 through a peripheral circuit containing Smad1, Smad6, and Runx1. Bmp4 affects the triad indirectly by regulating the Smad1 phosphorylation rate. Smad6 negatively regulates pSmad1 and Runx1 (blunted arrows) by targeting them for proteasomal degradation. Arrows represent positive transcriptional regulation. (B) Detailed representation of the regulatory connections in the GRN that explicitly shows the various promoters and binding sites (using the notation from (8)). The top half of the diagram shows the triad module, whereas the bottom half shows the signaling module.

Results

Notch1 is necessary for irreversible activation of the triad

Definitive hematopoiesis is the production of blood progenitor cells with the potential to form mature erythroid and myeloid cells, and occurs in multiple sites of the developing embryo including the yolk sac, placenta, AGM and head regions (Li et al., 2012; Lux et al., 2008; Medvinsky and Dzierzak, 1996; Rhodes et al., 2008). The Scl–Gata2–Fli1 triad (Fig. 1A, dashed box) is at the core of the GRN analyzed here; its activation with Notch1 and Bmp4 signals is known to play an important role in definitive hematopoiesis (Durand et al., 2007; Kataoka et al., 2011; Pimanda et al., 2007b; Wareing et al., 2012). Previously, we used a mathematical model to show that Notch1 and Bmp4 cause an irreversible switch to high levels of triad gene expression and thereby explained their role in the activation of these master regulatory genes of definitive hematopoiesis (Narula et al., 2010). Here we extend this model to incorporate recently uncovered interactions between components of the Bmp4 signaling pathway and Runx1, another key regulator of definitive hematopoiesis (Knezevic et al., 2011; Pimanda et al., 2007a).

In this extended model we explicitly include the components involved in Bmp4 signaling—Smad1, Smad6 and Runx1. We briefly outline the major interactions and assumptions of the model (see the "Methods" section and SI for details). Bmp4 promotes the phosphorylation of Smad1, following which pSmad1 translocates to the nucleus and upregulates the transcription of the triad genes as well as of Runx1 and Smad6 (Attisano and Wrana, 2002; Bee et al., 2009a; Ishida et al., 2000). Runx1 forms a complex with pSmad1 in the nucleus (Zaidi et al., 2002). We assume that the formation of this complex enhances the effect of pSmad1 on triad gene expression although it is not essential for triad upregulation. As a result, in our model, Runx1 participates in triad regulation but is not essential for triad gene expression. Smad6 post-translationally modulates Bmp4 signaling by forming complexes with Runx1 and pSmad1, and thereby targeting them for proteolytic degradation (Knezevic et al., 2011; Murakami et al., 2003). In addition the triad feeds back to the signaling module by transcriptionally upregulating Runx1, Smad6 and Smad1 (see the "Methods" and Fig. S1; (Bee et al., 2009a, 2009b; Knezevic et al., 2011; Nottingham et al., 2007; Pimanda et al., 2007b)). It should be noted that our model focuses specifically on the emergence of HSCs from the hemogenic endothelium and as such cannot be used to infer the effects of either Bmp4 and Notch1 signals or triad gene expression levels on the eventual fate (i.e. differentiation and/or proliferation potential) of these cells.

To understand the role of the Smad1–Smad6–Runx1 signaling module we first examine the steady-state response of the network to Notch1 and Bmp4 signals. To this end we compute how the steady-state concentrations of the triad proteins depend on the

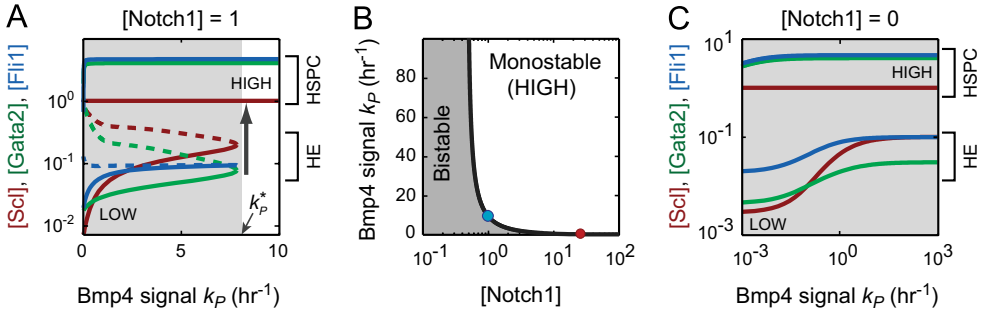

Fig. 2. Notch1 is necessary for triad activation. Steady-state concentrations of the triad proteins are plotted as a function of Smad1 phosphorylation rate, (k_p), a proxy for Bmp4 signal (panels A and B). Red, blue and green curves represent the steady-state concentrations of Scl, Gata2 and Fli1, respectively. Solid and dashed lines represent the stable and unstable states, respectively. Grey areas represent the region where the triad is bistable and can exist in either LOW or HIGH concentrations. (A) In the presence of Notch1, the triad LOW state only exists when Bmp4 signal is below a certain threshold (k_p^*). Signals above the threshold ($k_p > k_p^*$) irreversibly switch the triad to HIGH state (shown by arrow). In this and other figure panels HIGH and intermediate Scl concentrations represent HSPC (Hematopoietic Stem and Progenitor Cell) and HE (Hemogenic Endothelium), respectively. (B) Black curve shows the dependence of k_p^* on [Notch1]. Below this curve the triad is bistable, whereas above it the triad is monostable and can only exist in the HIGH state. Note that at very low [Notch1] the triad is always bistable. The blue dot shows the operating point [Notch1]=1 used in panel A. The red dot denotes the amount of Notch1 that can activate the network in the absence of a Bmp4 signal. (C) In the absence of Notch1, the triad can exist in either HIGH or LOW states, both of which exist and are stable for all values of the Bmp4 signal. (For interpretation of the references to color in this figure legend, the reader is referred to the web version of this article.)

signal levels. In our model the Smad1 phosphorylation rate (k_p) is used as a proxy for Bmp4 signaling (Kretzschmar et al., 1997), whereas Notch1 signaling is modeled explicitly as the binding of Notch1 to the Gata2 promoter site (Robert-Moreno et al., 2005). We find that the triad module is irreversibly bistable (Fig. 2) which is in line with our previous results (Narula et al., 2010). As a result, for a range of Notch1 and Bmp4 signals the triad can exist in one of two expression regimes: low expression (LOW) or high expression (HIGH) of all three triad genes. In both regimes, steady state expression levels of triad genes increases with increase in Notch1 and Bmp4 signal levels (Fig. 2A). In the presence of Notch1, the LOW state only exists when the Bmp4 signal is below a certain threshold (Fig. 2A, grey area). In this region the system is bistable, whereas outside (Fig. 2A, white area) the system is monostable and can exist only in the HIGH state. Therefore, increasing the Bmp4 signal irreversibly switches the triad from LOW to HIGH (indicated by arrow in Fig. 2A). The multiple positive feedback loops in the triad maintain it in the HIGH state even after the signals (Bmp4 and/or Notch1) are removed. This again is in accord with our previous results (Narula et al., 2010). It should be noted that due to the multiple cooperative interactions between the triad genes, at steady state all three triad gene are predicted to simultaneously be either in the LOW or HIGH expression states.

Although it not known what level of triad gene expression is required to facilitate the transition of a pre-hemogenic endothelial cell to a hemogenic endothelial (HE) cell we assume here that the irreversible switch from triad LOW to triad HIGH is not required for this transition and the increase in LOW state triad expression in response to Bmp4 is sufficient for transition to HE (Fig. 2A). Moreover, we believe that the irreversible switch that occurs past a threshold level of Bmp4 signal (hereafter referred to as the activation threshold, k_p^*) represents the transition of HE cells to Hematopoeitic Stem/Progenitor cells (HSPCs).

The model predicts that the Bmp4 signal threshold for triad activation (k_p^*) depends on the level of Notch1 (Fig. 2B, black curve). Increasing Notch1 lowers this activation threshold. For the parameter values used in the model, finite amounts of Notch1 result in triad activation even in the absence of Bmp4 signal (Fig. 2B, red dot). Thus, the model predicts that significant over-expression of Notch1 can lead to triad activation even in the absence of Bmp4 signal. On the other hand, decreasing Notch1 below a certain level causes the activation threshold to approach infinity, thereby making the activation impossible in the absence of Notch1. Fig. 2C shows that in the absence of Notch1 the triad is always bistable, i.e., both HIGH and LOW states exist, regardless of the Bmp4 signal level. As a result, while Bmp4 can cause an increase in triad gene expression it is impossible to switch the cells that start in the triad LOW state to HIGH state by increasing Bmp4 signal in Notch1 mutants. This prediction is consistent with the observation that blood progenitor emergence does not occur in the Notch1-null embryo proper (Hadland et al., 2004; Kumano et al., 2003).

The model explains accelerated emergence of HSCs in Runx1 heterozygotes

Next we analyze the role of Runx1 in triad activation. In the Runx1-null mutant (*Runx1*$^{-/-}$) the triad is bistable (Fig. 3A), and as with the Notch1-null mutant (Fig. 2C) both LOW and HIGH states exist regardless of the Bmp4 signal level. As a result, while Bmp4 can increase triad gene expression and lead to the appearance of the hemogenic endothelium (HE), it cannot cause the irreversible transition to HIGH state (HSPC) and cells remain stuck in the HE stage. This effect is related to Runx1's ability to enhance the transcription of triad genes by forming a nuclear complex with their regulator pSmad1 (Zaidi et al., 2002).

We further explore the effect of Runx1 on the triad in Fig. 3B by examining how activation threshold (k_p^*) changes with the maximum Runx1 production rate (v_r^o). As expected from Fig. 3A, Bmp4-mediated triad activation is not possible if the Runx1 production rate is below a minimum level (see Fig. S2). Increasing production rate above this minimal level has a non-monotonic effect (i.e. both increasing and decreasing) on the activation threshold. In this case the effect is first decreasing, then increasing and finally again decreasing (black–green–blue curve, Fig. 3B). This is a consequence of the contrasting roles that Runx1 plays in modulating triad activation—positive via complex formation with pSmad1 and negative via upregulation of Smad6. Initially, increasing Runx1 production rate decreases the activation threshold (black branch, Fig. 3B) due to the cooperative effect of Runx1 on pSmad1's up-regulation of the triad. However, an opposite trend is observed later where increasing Runx1 production rate increases the activation threshold (green branch, Fig. 3B) due to Runx1's negative effect on pSmad1 via up-regulation of Smad6-mediated degradation. Further increasing Runx1 production makes its level high enough to sequester all of Smad6, thereby saturating the negative effect on pSmad1. As a result, increasing Runx1 production rate

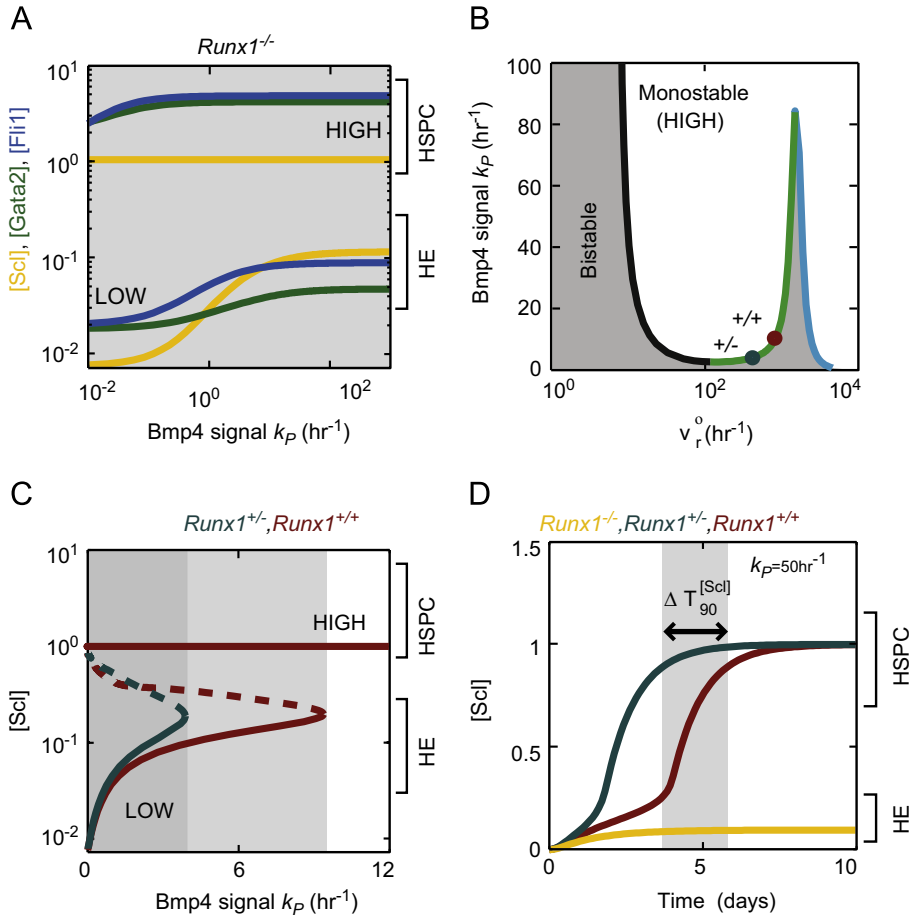

Fig. 3. The role of Runx1 in triad activation. (A) In the Runx1 null mutant (*Runx1*$^{-/-}$), the triad is bistable, but Bmp4 signaling is incapable of switching the triad from LOW to HIGH (HSPC). However triad expression can still increase leading to the appearance of HE. Red, blue, and green curves represent Scl, Gata2 and Fli1 concentrations, respectively. (B) Activation threshold (k_p^*) changes non-monotonically with increase in the Runx1 production rate (black–green–blue curve). Grey area represents the region where triad is bistable. Red and green dots denote the activation thresholds for WT (*Runx1*$^{+/+}$) and Runx1 haploid mutant (*Runx1*$^{+/-}$), respectively. (C) Steady-state response of triad to Bmp4 signal in WT (*Runx1*$^{+/+}$-red curve) and haploid mutants (*Runx1*$^{+/-}$-green curve). Only [Scl] is shown for clarity. The activation threshold for haploid *Runx1* mutant is ~1/2 of that for WT. Dashed curves show unstable states. (D) Dynamics of triad activation in response to a step-increase in Bmp4 signal from k_p=0 to k_p=50 h^{-1}. The dynamics depend on *Runx1* gene dosage. The lower activation threshold allows haploid mutant (green curve) to speed-up triad activation by ~2 days compared to WT (red curve). Grey region represents $\Delta T_{90}^{[Scl]}$, the difference in time to reach 90% of [Scl] level in HIGH state. Note that the *Runx1* null-mutant only switches to HE in the presence of the same signal (yellow curve). (For interpretation of the references to color in this figure legend, the reader is referred to the web version of this article.)

decreases the Bmp4 signal required for triad activation (blue branch, Fig. 3B).

For model simulations, we assume that wild-type Runx1 (WT, *Runx1*$^{+/+}$) production rate lies in the intermediate portion of the curve in Fig. 3B (red circle). Hence, a reduction in Runx1 production rate lowers the activation threshold. This model assumption is crucial to explain the phenotype observed in Runx1 heterozygous deletion mutants (*Runx1*$^{+/-}$). In *Runx1*$^{+/-}$ mutants there is a 50% decrease in Runx1 production rate (green circle, Fig. 3B), due to which the activation of the triad can occur at a lower Bmp4 signal threshold (compare k_p^* for red and green circles in Fig. 3B). Comparing the steady-state triad responses reveal that the activation threshold for *Runx1*$^{+/-}$ mutant is ~1/2 of that for the WT (Fig. 3C). This decrease greatly affects the dynamics of triad activation.

Runx1 is known to be essential for HSC emergence, however surprisingly HSC emergence is accelerated in the *Runx1*$^{+/-}$ mutants (Cai et al., 2000; Lacaud et al., 2004). To understand this difference in the dynamics of HSC emergence between WT and *Runx1*$^{+/-}$ mutant we simulate the kinetics of triad LOW-to-HIGH activation. Specifically, we study the kinetics of triad activation in response to a step-up in the Bmp4 signal (k_p) to a value exceeding the WT activation threshold (five times the value of k_p^* for the red circle in Fig. 3B). As shown in Fig. 3D, the decrease in the activation threshold for the *Runx1*$^{+/-}$ mutant (observed in Fig. 3B and C) results in much faster activation of the triad. The speed-up in the activation can be quantified by $\Delta T_{90}^{[Scl]}$—the difference in the times between WT and haploinsufficient mutant at which Scl reaches 90% of its HIGH steady state value. For the chosen parameter values, $\Delta T_{90}^{[Scl]}$ is about 2 days, which is in quantitative agreement with the experimental observation that HSC emergence occurs earlier in *Runx1*$^{+/-}$ embryos (Cai et al., 2000; Lacaud et al., 2004). Though the precise value of $\Delta T_{90}^{[Scl]}$ is affected by changes in kinetic parameters the qualitative effect is robust (Figs. S3 and Text S1) as it is a consequence of a fundamental property of bistable switches —critical slowdown in dynamics near ghost steady states (Fontich and Sardanyes, 2008; Tiwari et al., 2010; Tiwari and Igoshin, 2012).

Runx1 overexpression can compensate for Notch1 deletion

Recent in vitro experiments have shown that artificially-induced Runx1 overexpression can rescue definitive hematopoiesis in Notch1 null mutants (Nakagawa et al., 2006). To mimic this experiment and to understand the relationship between Runx1 and Notch1 in the context of HSC emergence we introduce an additional Runx1 production term (v_{rr}) in our model (see the "Methods" section and SI). Simulations show that, similar to its dependence on v_r^o, the activation threshold k_p^* changes

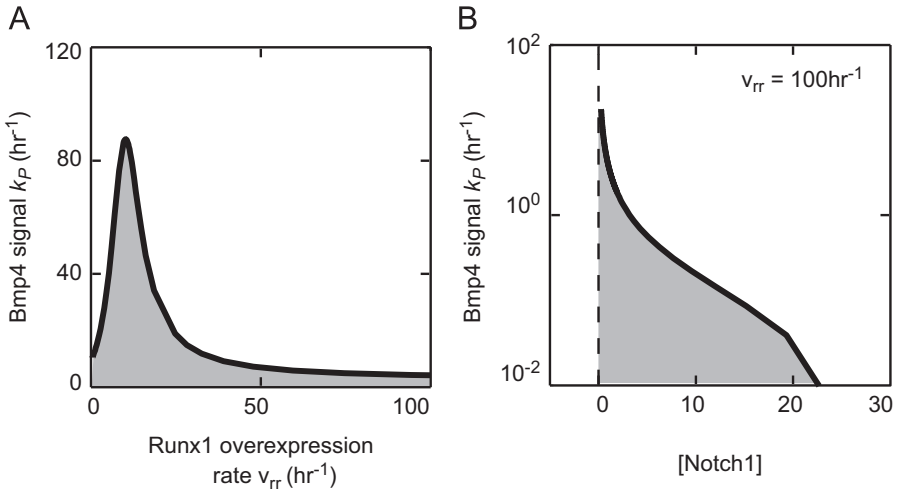

Fig. 4. Runx1 overexpression compensates for Notch1 deletion. (A) k_p^* changes non-monotonically as a function of Runx1 overexpression rate v_{rr} (black curve). (B) At high v_{rr}, Notch1 is not essential for Triad activation as indicated by a finite value of k_p^* (black curve) at [Notch1]=0.

non-monotonically as a function of the Runx1 overexpression rate v_{rr} (black curve, Fig. 4A). To uncover the consequences of Runx1 overexpression, we fix v_r^o at the level shown in Fig. 3B and choose a high v_{rr} (=100 h^{-1}). We find that this level of Runx1 overexpression allows the triad to be activated by Bmp4 signal alone ([Notch1]=0 results in finite k_p^* in Fig. 4B; compared to Fig. 2B). Therefore, our model explains the observation in Nakagawa et al. (2006) that artificially-induced Runx1 overexpression rescues definitive hematopoiesis in Notch1-null mutants by reducing the activation threshold to physiologically relevant levels.

Timing of Runx1 conditional deletion or Smad1 overexpression determines triad activation dynamics

Several studies have used Cre-mediated recombination and induced overexpression to highlight the dynamical roles of the Bmp4-signaling circuit components Smad1 and Runx1 in definitive hematopoiesis (Chen et al., 2009; Lacaud et al., 2002; Tanaka et al., 2012; Zafonte et al., 2007). In particular, these studies have shown that (i) Runx1 is only essential up to a certain stage in HSC emergence and can be conditionally deleted after this stage without compromising HSC maintenance (Chen et al., 2009; Lacaud et al., 2002) and (ii) transiently induced artificial overexpression of Smad1 expands hematopoietic progenitor populations only in a specific time-window of HSC emergence (Zafonte et al., 2007). These studies shed light on previously unknown dynamical properties of the regulatory system controlling hematopoiesis, however, the mechanistic underpinnings of the transient roles of Runx1 and Smad1 remain unexplained. We use our model to show that these transient roles are the result of the dynamical characteristics of the irreversible bistability in the triad.

First, we address the recent observations that only transient expression of Runx1 is required for HSC emergence (Chen et al., 2009; Lacaud et al., 2002; Tanaka et al., 2012). In Chen et al. (2009), Runx1 was conditionally deleted at different stages of early embryonic development, and it was found that if this deletion occurs sufficiently early, HSCs never emerge (Chen et al., 2009). However, if Runx1 was conditionally deleted later in the developmental process HSC emergence is unaffected. Similar temporal and cell state requirements for Runx1 were observed using different techniques in other studies, including recent work demonstrating that Runx1 activity is required at E7.5, four days prior to HSC emergence at E11 (Lacaud et al., 2002; Tanaka et al., 2012). To explain these experiments we simulate the activation of the triad (only Scl shown in Fig. 5A) to a step-increase in Bmp4 signal and then decrease the Runx1 production rate to zero at different times (12 h, 24 h,. etc). Our model shows that if Runx1 is knocked out after triad proteins reach sufficient levels for self-activation, there is negligible impact on the triad's steady state or dynamic behavior (Fig. 5A and Fig. S4). This is a consequence of the characteristic property of irreversibly bistable switches that they only require transient activation to switch to the HIGH state. Once the triad proteins reach sufficient levels (the region of attraction for the HIGH state), the positive feedback loops in the triad forces the system to quickly reach the HIGH state irrespective of the signal level. Our model shows a distinct time threshold of about 3.5 days, thereby defining how long Runx1 expression is necessary for triad activation and hence HSC emergence (Fig. 5B and Fig. S4). Therefore, our model is able to quantitatively capture the transient requirement of Runx1 during HSC emergence (Chen et al., 2009).

The effects of a pulse of Smad1 overexpression on the dynamics of hematopoietic progenitor cell emergence in vitro has been recently described (Zafonte et al., 2007). The results indicated that this effect depends non-monotonically on the timing of the Smad1 overexpression pulse. We simulate this experiment *in silico* by including an additional Smad1 production term (rate of production −0.1 h^{-1}) in our model equations. Consistent with the experimental protocol, this additional production is only active for a 6-h period starting at a specific time-point in the simulation. Under these modifications, we vary the time of Smad1 overexpression pulse and analyze the triad activation dynamics in response to a step-increase in Bmp4 signal. Fig. 5C shows the Scl activation dynamics in the presence (black, green and yellow curves) and absence of pulses (red curves). Blue bars depict the Smad1 pulse timing. The difference in time to reach 90% of the final Scl concentration with and without a pulse, $\Delta T_{90}^{[Scl]}$, is denoted by grey regions. Our model shows that early (~day 0—top panel) and late pulses (~day 4—bottom panel) have small effects on triad activation dynamics whereas a pulse of Smad1 around day 2 (middle panel) considerably speeds-up Scl activation (Fig. 5C). This non-monotonic dependence of triad activation speed-up ($\Delta T_{90}^{[Scl]}$) on the timing of the Smad1 pulse (Fig. 5D) could explain why Smad1 pulses only expand the hematopoietic progenitor population within a limited developmental time window (Zafonte et al., 2007). This non-monotonic dependence is a consequence of the characteristic slow-down in switching dynamics of a bistable switch. Bistable systems are known to slow-down in a critical concentration range during a switch between states (Fontich and Sardanyes, 2008; Sciammas et al., 2011). The coordination of a Smad1 pulse with the time at which the triad reaches the critical

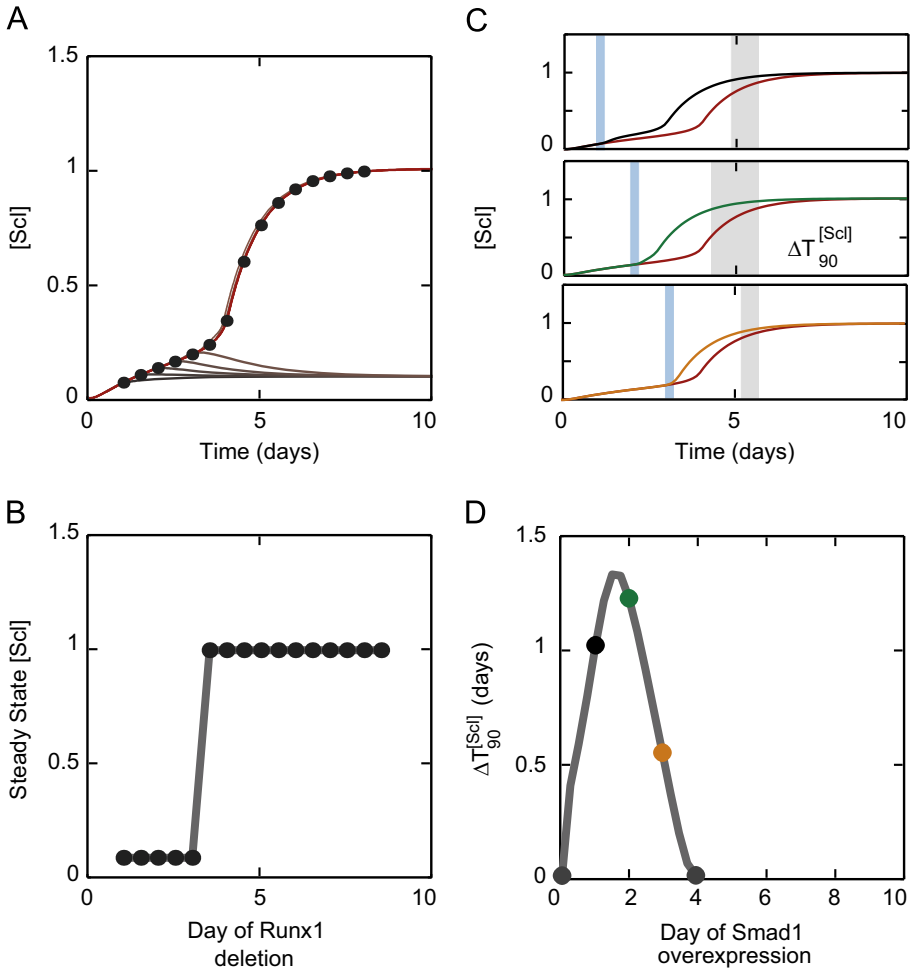

Fig. 5. Timing of Runx1 conditional deletion or Smad1 overexpression determines whether Triad activation is affected or not. (A) Scl dynamics with different timings of *Runx1* conditional deletion. Each black circle denotes the time in the trace at which Runx1 production is reduced to zero. Brown curves show Scl dynamics for systems that fail to activate due to *Runx1* conditional deletion, whereas red curves represent activated systems. Switch to HIGH state of the triad with Bmp4 signaling is impossible if *Runx1* is deleted early; however, cells can still increase Scl expression and reach the HE stage. *Runx1* deletion after a certain time has negligible effect on triad activation dynamics or final steady state. (B) Steady-state Scl concentration as a function of the time of *Runx1* conditional deletion. Early *Runx1* deletion interferes with triad activation and cells cannot fully upregulate Scl; however, *Runx1* deletion after day 3.5, has no effect on triad activation. (C) Scl dynamics with different timing of a Smad1 overexpression pulse. Smad1 is overexpressed at a rate of 0.1 h^{-1} for a 6 h time-window at specific times during triad activation. Red trajectories show Scl dynamics without Smad1 overexpression. Blue bars indicate the times of Smad1 overexpression for other trajectories. Note that overexpression around day 2 (middle panel) speeds-up triad activation the most, whereas both early and late overexpression have less prominent effects (top and bottom panels). Grey region represents the difference in time to reach 90% of the final [Scl], $\Delta T_{90}^{[Scl]}$, with and without the pulse. (D) Speed-up of triad activation $\Delta T_{90}^{[Scl]}$, depends non-monotonically on the time of Smad1 overexpression. (For interpretation of the references to color in this figure legend, the reader is referred to the web version of this article.)

slow-down concentration range can significantly speed-up the dynamics. However due to the small pulse duration, pulses that are timed to occur before the triad reaches this region have little effect on the overall time to reach the steady state. Pulses that come after the triad has passed the slow-down have already been delayed in the critical region and again the contribution to activation time is expected to be small.

Novel predictions about the roles of Runx1 and Smad6 in HSC emergence

Based on the non-monotonic relationship between Runx1 expression rate and triad activation threshold (see Fig. 3B) we can make several predictions about the roles of Runx1 and Smad6 in this master-regulatory circuit controlling HSC emergence. Our model predicts that unlike the WT, in Smad6-null mutants the dynamics of HSC emergence will be identical in $Runx1^{+/-}$ and $Runx1^{+/+}$ backgrounds (see Fig. S5A–C). In addition, we predict that stabilization of *p*-Smad6 activity by inhibiting its proteasomal degradation by Bortezomib (Mukherjee et al., 2008) would neutralize the proteolytic effect of Smad6 on Runx1 thereby reducing the difference between HSC emergence dynamics in $Runx1^{+/+}$ and $Runx1^{+/-}$ mutants (see Fig. S5D and E). Finally, we note that, relative to WT, a mutant with three copies of Runx1 is predicted to increase Smad6 expression and consequently the triad activation threshold. As a result, HSC emergence in triploid Runx1 mutants is expected to be slower than both WT and $Runx1^{+/-}$ mutants (Fig. S5F).

Discussion

We have developed a comprehensive model for the network controlling definitive blood emergence by combining our previous model (Narula et al., 2010) of the Scl–Gata2–Fli1 triad with the Bmp4 signaling module containing Smad1, Smad6 and Runx1. This framework allows us to systematically assess, analyze and predict the effects of perturbations on dynamical properties of this network. The model shows that the GRN module under consideration is irreversibly bistable and can be activated by the combination of

Notch1 and Bmp4 signaling. Once activated, the triad remains active even when the signals are removed. If high levels of Scl–Gata2-–Fli1 gene expression ensure a stable HSC state, the irreversible activation of the triad in the AGM could explain why Bmp signaling later becomes dispensable for the maintenance of HSCs in the fetal live and adult bone marrow (Singbrant et al., 2010). We have hypothesized that the irreversible activation of this bistable switch is not required for the formation of hemogenic endothelial cells but occurs in HE cells and both contributes to and is modulated by Runx1 expression which plays a critical role in the emergence of blood stem/progenitors from the HE. It is important that this irreversible bistable switch occurs prior to blood cells emerging from the HE so that maximal expression of these factors, which are required for down-stream applications, is achieved prior to cells losing resident cues from their tissues of origin. Based on this hypothesis, we can compare the predicted dynamical properties with those observed in various in vivo and in vitro genetic perturbations of this network.

Our model predicts that Runx1 is essential for definitive hematopoiesis in part because it mediates Bmp4 signaling and is required, albeit only transiently, for the activation of the triad module. Moreover, the model is able to reconcile this essential requirement of Runx1 for definitive hematopoiesis (Lacaud et al., 2002) with the counter-intuitive observation that heterozygous deletion of Runx1 actually accelerates HSC emergence (Cai et al., 2000; Lacaud et al., 2004). We have predicted that this acceleration is connected to the negative effect that Runx1 has on pSmad1 levels via upregulation of Smad6. Due to this negative effect, the two-fold decrease in the Runx1 production rate that results from a heterozygous deletion decreases the Bmp4 signal threshold and thereby accelerates triad activation. Based on our simulations we also predict that when examined in a Smad6-null mutant background or in the presence of specific proteasome inhibitors, there will be little or no difference in dynamics of HSC emergence between $Runx1^{+/+}$ and $Runx1^{+/-}$.

Additionally, the model predicts that the transient perturbations to the signaling module will affect the activation dynamics only if they occur sufficiently early. Current observations of the temporal requirement for Runx1 during hematopoietic development suggest it is required early, either in the E7.5 extra-embryonic mesoderm, and/or later in the hemogenic endothelium (Tanaka et al., 2012). We predict that the conditional deletion of Runx1 has no effect on triad activation if it occurs after ~3.5 days from the onset of the hematopoietic program. We also predict that pulsed overexpression of Smad1 leads to the expansion of the hematopoietic progenitor population within a particular time-window and the magnitude of the expansion depends non-monotonically on the timing of the Smad1 pulse. These predictions are in excellent qualitative and quantitative agreement with recently reported and unexplained experimental observations that motivated these simulations (Chen et al., 2009; Tanaka et al., 2012; Zafonte et al., 2007). Moreover, these predictions are robust to the parameter values used in the model as these dynamical effects are related to the fundamental mathematical properties of bistable switches (see Text S1 Figs. S3, S4).

We have also found that these predictions are robust to certain changes in the dynamics of upstream signaling systems such as the Notch pathway. While this manuscript was under review, a new study has shown that Notch signaling is downregulated during HSC emergence (Richard et al., 2013). By repeating our simulations for a decreasing Notch1 level (see Text S1), we found that this change in the dynamics of Notch signaling increases the minimum Bmp4 signal required to switch the triad to a high expression HSC state (Fig. S6A and B). However decreasing Notch1 levels do not change our results regarding the earlier emergence of HSCs in the haploid $Runx1^{+/-}$ mutants (Fig. S6C and D). This shows that our predictions are qualitatively robust to dynamical changes in the signaling systems controlling the HSC network.

In our model we have used a statistical thermodynamics framework (Bintu et al., 2005; Mirny, 2010; Narula et al., 2010) to model the combinatorial effect of multiple transcription factors on gene regulation. Following recent experimental evidence (Knezevic et al., 2011; Narula et al., 2010; Nottingham et al., 2007; Oren et al., 2005; Pimanda et al., 2007a, 2007b), we assume that transcription factors acting at *cis*-regulatory elements control gene expression by increasing the probability of a RNA-polymerase accessible state of chromatin rather than through direct physical interactions with polymerase (see the "Methods" section). This no-contact assumption posits a biophysical mechanism for gene regulation which is different from the typical TF-RNA polymerase contact mechanism where DNA looping is assumed (Bintu et al., 2005). However, mathematically the two approaches are interconvertible (see the "Methods" section) and the no-contact mechanism dramatically reduces the number of free model parameters and thereby enhances the utility of this approach when data is limited.

The heterogeneity of assays and functional readouts of definitive blood development limits the direct comparisons between model predictions and experimental data. Nevertheless we have demonstrated that predictions from our model are consistent with experimental observations. Altogether our model shows that the temporal influence of Runx1 and mediators of the Bmp4 signaling pathway on the emergence of HSCs and progenitor cells can be explained by their effects on the activation dynamics of the Scl–Gata2–Fli1 triad. Such an integrative view of the GRN controlling definitive blood cell emergence offers a way to consolidate information from an array of genetic perturbation experiments. Nevertheless it should be noted that while this model reflects and explains current knowledge of HSC emergence in the AGM it will require updating to accommodate future advances in our knowledge. However, as Fig. S6 demonstrates, our qualitative predictions can be robust to the incorporation of newly discovered features of signaling dynamics (Richard et al., 2013) whereas some quantitative predictions remain sensitive to these changes.

Our model also enables us to generate hypotheses about the roles of network components and connections. For instance, our observation that higher Runx1 production rates lead to slower emergence (Fig. 3D), may indicate that Runx1 plays a role in the temporal order of stem/progenitor emergence from hemogenic endothelium during embryonic development, i.e. progenitors with restricted lineage potential preceding emergence of definitive HSCs.

Although required for definitive HSC production, neither Runx1 nor Notch1 is essential for primitive erythroid development, whereas components of the triad such as Scl are required for both (Lacaud et al., 2002; Robb et al., 1995; Shivdasani et al., 1995). Our view is that activation of the triad to the HIGH state may not be essential for primitive hematopoiesis. As such, expression of components of the triad (such as Scl) which are required for this process can occur without activation of the triad to the HIGH state. In this context, our model shows that although Runx1 and Notch1 are essential for switching the triad to the HIGH expression state of the HSCs, Bmp4 can lead to increased expression of triad components in their absence (Fig. 3A).

Conclusion

Despite much advancement in our understanding of how HSCs are formed in the embryo, translating this knowledge into novel protocols for the in vitro production of HSCs has proved difficult due to the complexity of the network architecture that control this

process. Our results demonstrate that despite this complexity, computational approaches are a useful adjunct to integrating experimental data and help interpret previously unexplained biological observations on dynamical network properties. The model proposed here suggests two issues that may influence future protocol design; the first is the importance of signal pathway combinatorial activity, demonstrated by the complementary roles of Notch1 and Bmp4; and the second is the vital role of negative regulators such as Smad6 in fine-tuning the levels of key transcription factors (also relevant given the recent findings describing a Notch, Hes1 and Gata2 network with negative feedback (Guiu et al., 2013)). Both issues could inform how the duration and combination of exogenous stimulation of key signaling pathways is considered when developing future HSC production protocols.

Methods

Mathematical model for the gene regulatory network containing triad and signaling modules

To uncover the role of Runx1, Smad1 and Smad6 in hematopoietic stem cell (HSC) emergence we use an ordinary differential equation (ODE) based deterministic model. This model is based on known transcriptional and post-translational interactions (see Fig. 1) and previously published experimental characterizations of the various *cis*-regulatory interactions in the network controlling HSC emergence in the embryo. These are described in detail in the following sections.

Thermodynamic modeling of gene regulation

We combine the processes of transcription and translation involved in the production of a protein from its corresponding gene into a single synthesis reaction. The rate of this reaction depends on the combinatorial binding of transcription factors (TFs) at promoters and enhancers that regulate the expression of each gene. Further, we assume based on available experimental results (Pimanda et al., 2007b; Smith et al., 2008) that the increase in the transcriptional rate occurs via modulation of the state of chromatin rather than through direct interaction with transcriptional machinery. We call this the No-contact model of transcriptional regulation by *cis*-regulatory elements (Mirny, 2010; Narula and Igoshin, 2010; Narula et al., 2010) as opposed to Contact models where transcription factors act by direct physical interaction with RNA polymerase. Specifically, the gene of interest can exist in either a RNA polymerase-accessible (open) chromatin or RNA polymerase-inaccessible (closed) chromatin state. The binding of TFs at the enhancer or promoter shifts the equilibrium towards the open state, thereby increasing the probability of gene expression. As a result, the probability of transcription can be approximated by the probability of the open chromatin state. To determine how this probability depends on the concentrations of various TFs we use a statistical thermodynamic approach (Mirny, 2010; Narula and Igoshin, 2010; Narula et al., 2010) that allows us to derive each gene's regulatory function on the basis of known combinatorial interactions. The parameterization of such a regulatory function requires measurements of binding affinities between DNA and TFs as well as interaction strengths among TFs. This entails measuring the contribution of each TF to the transcriptional rate, both individually as well as in every possible combination with other TFs. It is extremely difficult to measure all these contributions due to the combinatorial multiplicity of TF configurations at enhancers and promoters in eukaryotic systems, and as a result such information does not exist for most systems. Instead, experimental data typically includes quantification of the effect of mutation of specific TF binding sites on the expression rates from a luciferace or *lacZ* reporter (Narula et al., 2010; Pimanda et al., 2007b). Previously, we have shown that such measurements can be used to estimate the strengths of TF–TF and TF–DNA interactions by using appropriate normalization for TF concentrations (Narula et al., 2010). Here we use the same methods to model the GRN in Fig. 1 and to estimate the various parameters. Below we provide the various regulatory functions and estimated parameter values, however we refer the reader to Narula and Igoshin (2010), Narula et al. (2010) for details of this method and provide the regulatory functions and parameters used in our model below.

Relationship between no-contact and contact models of transcriptional regulation

Consider a gene Y regulated by the combinatorial action of multiple activating TFs X_i ($i\in 1,2,\ldots,n$) at a *cis*-regulatory region. In the no-contact model (see Narula and Igoshin, 2010 for a detailed derivation), the transcription rate of Y can be written in terms of the concentrations of X_is:

$$v_Y = v_Y^o \frac{z_Y}{(K_Y + z_Y)};$$
$$z_Y = 1 + \sum_{i=1}^{n} [X_i] e^{-G_i} + \sum_{i=1}^{n}\sum_{j=1}^{n} [X_i][X_j] e^{-G_{ij}} + \cdots \quad (1)$$

where v_Y^o is the maximum rate of expression of gene Y, K_Y is the equilibrium constant of chromatin remodeling, $[X_i]$ is the concentration of TF i, and G_i is the binding free energy of TF i. The fraction $z_Y/(K_Y+z_Y)$ is the probability of the RNA-polymerase accessible state of chromatin and its exact form is determined by the partition function z_Y which sums over all the possible TF-bound states of the regulatory region. In this model we assume that TFs only control the probability of the polymerase accessible state of chromatin at the promoter and therefore the rate of transcription is proportional to the probability of finding DNA in one of the accessible conformations. In this mechanism, regulation of transcription by TFs does not require their physical interaction with RNA polymerase. However, as shown below, the regulatory function of this No-contact mechanism (Eq. (1)) can be rewritten in a form similar to regulatory functions for a contact mechanism of gene regulation where TFs do interact with RNA polymerase.

Dividing both numerator and denominator in Eq. (1) by K_Y+1 we obtain,

$$v_Y = \frac{v_Y^o}{K_Y + 1} \frac{1 + \sum_{i=1}^{n} [X_i] e^{-G_i} + \sum_{i=1}^{n}\sum_{j=1}^{n} [X_i][X_j] e^{-G_{ij}} + \cdots}{1 + \sum_{i=1}^{n} [X_i] \frac{e^{-G_i}}{K_Y+1} + \sum_{i=1}^{n}\sum_{j=1}^{n} [X_i][X_j] \frac{e^{-G_i}}{K_Y+1} + \cdots} \quad (2)$$

The above equation can be rewritten as

$$v_Y = v_Y^{basal} \frac{1 + \sum_{i=1}^{n} f[X_i] e^{-G'_i} + \sum_{i=1}^{n}\sum_{j=1}^{n} f[X_i][X_j] e^{-G'_{ij}} + \cdots}{1 + \sum_{i=1}^{n} [X_i] e^{-G'_i} + \sum_{i=1}^{n}\sum_{j=1}^{n} [X_i][X_j] e^{-G'_{ij}} + \cdots} \quad (3)$$

where

$$v_Y^{\text{basal}} = \frac{v_Y^o}{K_Y + 1}, \quad G'_i = G_i + \log(K_Y + 1) \quad \textit{and} \quad f = K_Y + 1,$$

Here the fold-change f can be interpreted as the maximum increase in transcription rate resulting from the binding of each TF or TF complex. Eq. (3) resembles the typical *cis*-regulatory function derived in the contact models of combinatorial transcription regulation where TFs directly interact with RNA polymerase (Bintu et al., 2005). As seen from Eqs. (2) and (3) the contact and no-contact models are mathematically equivalent even though they represent different biophysical mechanisms of gene regulation. However, in the contact model the fold-changes

resulting from binding of different TFs or TF complexes can be different but Eqs. (2) and (3) are only mathematically equivalent only under the assumption of equal fold-changes. It should be noted though that the experimental data that is generally available (measurements of *lacZ* expression from deletion libraries of *cis*-regulatory elements) is usually insufficient to simultaneously determine the fold-changes and binding free-energies of TFs and TF complexes (Narula and Igoshin, 2010; Narula et al., 2010). Therefore, we believe that using the no-contact model with its implicit assumption of equal fold-changes is a reasonable approximation. This formulation (Eq. (1)) is used throughout the following sections to derive the *cis*-regulatory functions of various genes in our model.

Notation

The notation used throughout these Methods is summarized in Table S1. Brackets $[\cdots]$ denote concentrations. Note that all concentrations are in dimensionless units and are assumed to be normalized by their steady-state values in the absence of Bmp4 and Notch1 signals. In addition, G_y^x, denotes a free energy of binding of TF x to an enhancer of gene y.

Triad transcriptional regulation

The triad genes Scl, Gata2 and Fli1 regulate each other by acting at the *Scl+19*, *Gata2–3* and *Fli1+12* enhancers (Pimanda et al., 2007b; Smith et al., 2008). In addition, the Gata2 promoter is known to be regulated by Bmp4 (via pSmad1) and Notch1 and the Fli1 promoter is regulated by Bmp4 (via pSmad1). Using available details of TF binding sites in these of enhancers and promoters we have previously shown that the following equations can be used to describe the rates of transcription v_s (Scl), v_g (Gata2) and v_f (Fli1) for the triad:

$$v_s = v_s^o \frac{z_s}{(K_s + z_s)};\quad z_s = 1 + [G]e^{-G_s^g} + [F]^2 e^{-2G_s^f} + [G][F]^2 e^{-G_s^{gf}} \tag{4}$$

$$v_g = v_g^o \frac{(1 + f_1([pS1{-}R] + \alpha[pS1])e^{-G^{bp}} + f_2[N1])z_g}{(K_g + (1 + ([pS1{-}R] + \alpha[pS1])e^{-G^{bp}} + [N1])z_g)};\quad z_g = 1 + [G]e^{-G_g^g} + [F]^2 e^{-2G_g^f} + [G][F]^2 e^{-G_g^{gf}} + [S][G][F]^2 e^{-G_g^{sgf}} \tag{5}$$

$$v_f = v_f^o \frac{(1 + f_1([pS1{-}R] + \alpha[pS1])e^{-G^{bp}})z_f}{(K_f + (1 + ([pS1{-}R] + [pS1])e^{-G^{bp}})z_f)};\quad z_f = 1 + [G]e^{-G_f^g} + [F]^2 e^{-2G_f^g} + [G][F]^2 e^{-G_f^{gf}} + [S][G][F]^2 e^{-G_f^{sgf}} \tag{6}$$

Here, v_s^o, v_g^o and v_f^o are the maximum rates of transcription from the Scl, Gata2 and Fli1 promoters in the absence of Notch1 and Bmp4 signals. K_s, K_g and K_f are the equilibrium constants of the chromatin state of the Scl, Gata2 and Fli1 regulatory regions, respectively. f_1 (=4) (Lugus et al., 2007) and f_2 (=3.5) (Robert-Moreno et al., 2005) denote the fold-change in gene expression rate resulting from the effect of Bmp4 and Notch1 on the appropriate promoters. Based on Oren et al. (2005), Zaidi et al. (2002), we have modified Eqs. (4)–(6) from those in Narula et al. (2010) to specify that Bmp4 affects Gata2 and Fli1 expression via the binding of pSmad1 and pSmad1:Runx1 complex. We assume based on the observations of Zaidi et al. (2002) that the pSmad1:Runx1 complex is more effective than pSmad1 alone at increasing the transcription from Gata2 and Fli1 promoters. Accordingly, we assume that pSmad1 alone can only effect a fold-change αf_1 where $\alpha < 1$. [N1] represents the concentration of Notch1 acting on the Gata2 promoter normalized by its dissociation constant of binding to the promoter. The parameters used in Eqs. (4)–(6) were derived in Narula et al. (2010) based on the results from Gottgens et al. (2002), Pimanda et al. (2007b) and are reproduced in Table S2.

Smad1 transcriptional regulation

Gene expression from the Smad1 promoter is regulated by the *Smad1–7* upstream enhancer. This enhancer includes multiple Fli1 (Ets) binding sites as well as a Gata2 binding site (Fig. S1 and data not shown). We assume that this enhancer modulates Smad1 transcription by controlling the probability of transcription from the Smad1 promoter. Following this assumption and the deletion analysis of the *Smad1–7* enhancer (Fig. S1) the rate of Smad1 transcription, v_{s1}, was modeled using the following equation:

$$v_{s1} = v_{s1}^o \frac{z_{s1}}{K_{s1} + z_{s1}};\quad z_{s1} = (1 + [F]^2 e^{-2G_{s1}^f})(1 + [F]e^{-G_{s1}^f})(1 + [G]e^{-G_{s1}^g}) \tag{7}$$

Here, v_{s1}^o is the rate of transcription from the Smad1 promoter and K_{s1} is the equilibrium constant of the chromatin state of the Smad1 regulatory region. Using lacZ-reporter expression assay data (not shown) we have determined the various free energies in Eq. (7) in terms of the K_{s1}. The parameter values used in model for the *Smad1–7* enhancer are given in Table S3.

Smad6 transcriptional regulation

Smad6 expression is regulated by the Smad6 promoter as well as the upstream *Smad6–57* enhancer (Fig. S1). Both the promoter and enhancer include binding sites for the triad proteins as well as Runx1 and pSmad1. We assume that this enhancer modulates the probability of transcription whereas the promoter controls the rate of Smad6 transcription. Following these assumptions and the deletion analysis of the Smad6 enhancer and promoter (Knezevic et al., 2011; Pimanda et al., 2007a), the rate of Smad6 transcription, v_{s6}, was modeled using the following equation:

$$v_{s6} = v_{s6}^o \frac{z_{s6p}}{(K_{s6p} + z_{s6p})} \frac{z_{s6e}}{(K_{s6e} + z_{s6e})};\quad z_{s6p} = (1 + [F]^2 e^{-2G_{s6p}^f})(1 + ([R] + [pS1{-}R])e^{-G_{s6p}^r})(1 + [S]^2[G][F]^2 e^{-G_{s6p}^{sgf}}),\quad z_{s6e} = 1 + [R]e^{-G_{s6e}^r}(1 + [G]e^{-G_{s6e}^g}) \tag{8}$$

Here, v_{s6}^o is the maximum rate of transcription from the Smad6 promoter and K_{s6p} and K_{s6e} are the equilibrium constants of the chromatin state of the Smad6 promoter and enhancer, respectively. Using the data from (Knezevic et al., 2011; Pimanda et al., 2007a) we can determine the various free energies in Eq. (8) in terms of K_{s6p} and K_{s6e}. The parameter values used in model for the Smad6 regulation are given in Table S4.

Runx1 transcriptional regulation

Runx1 expression is regulated by the two promoters P1 and P2 as well as the intronic *Runx1+23* enhancer (Fig. S1; (Bee et al., 2009a, 2009b; Nottingham et al., 2007; Pimanda et al., 2007a)). These promoters and enhancer include binding sites for the triad proteins as well as Runx1 and pSmad1. It has been shown that the *Runx1+23* enhancer specifically directs gene expression from both promoters in hemogenic tissue (Bee et al., 2009a). Moreover *Runx1+23* can modulate the gene expression from each promoter independent of the other (Bee et al., 2009b). It has also been recently shown that transcription from promoter P1 largely depends on the binding of Runx1 and pSmad1 rather than triad proteins (Bee et al., 2009a). We again assume that the enhancer modulates the probability of transcription whereas the promoters

control the rate of Runx1 transcription. Taking all these facts and assumptions into account and using the deletion analyses of the Runx1 enhancer and promoters (Bee et al., 2009a, 2009b; Nottingham et al., 2007; Pimanda et al., 2007a), the rate of Runx1 transcription, v_{s6}, was modeled using the following equation:

$$\begin{aligned} &v_r = v_r^o\left[\frac{z_{rp1}}{K_{rp1}+z_{rp1}}+\frac{z_{rp2}}{K_{rp2}+z_{rp2}}\right]\frac{z_{re}}{(K_{re}+z_{re})};\\ &z_{rp1}=1+[pS1{-}R]e^{-G^{ps1}_{rp1}}, z_{rp2}=1+[F]^2e^{-2G^{f}_{rp2}},\\ &z_{re}=1+[R][G]e^{-G^{rg}_{re}}(1+2[F]e^{-G^{f'}_{re}}+[F]^2e^{-2G^{f}_{re}}) \end{aligned} \tag{9}$$

here, v_r^o is the maximum rate of transcription from the Runx1 promoter and K_{rp1}, K_{rp2} and K_{re} are the equilibrium constants of the chromatin state of the promoters P1 and P2 and the *Runx1+23* enhancer, respectively. We assume the same v_r^o for both promoters since transcription from both promoters has been shown to be comparable (Bee et al., 2009a). Using the data from Bee et al. (2009a, 2009b), Nottingham et al. (2007), Pimanda et al. (2007a), we can determine the various free energies in Eq. (9) in terms of K_{rp1}, K_{rp2} and K_{re}. The parameter values used in model for the Runx1 regulation are given in Table S5. v_r^o was multiplied by 0, 0.5 and 1.5 to model mutations such as Runx1$^{-/-}$, Runx1$^{+/-}$ and three copies of Runx1, respectively.

Protein degradation/dilution

We assume that the rate of degradation for all model species follows first-order kinetics. Degradation rates k^i_{deg} for each species i in the model were calculated based on experimental data about protein stability (Yen et al., 2008). We used a half-life of 24 h for Scl, 4 h for Fli1 and 2 h for the remaining species (Gata2, Smad1, pSmad1, Runx1, Smad6, pSmad1:Runx1, pSmad1:Smad6 and Runx1:Smad6).

Post-translational reactions

The Bmp4 signaling network includes many post-translational interactions involving the regulatory Smads, Smad1 as well as the inhibitory Smad, Smad6 (Hata et al., 1998; Murakami et al., 2003; Zhang et al., 2001). Phosphorylation of Smad1 by Bmp4 bound receptors leads to the formation of pSmad1 which translocates into the nucleus and affects gene expression of Bmp4 signaling target genes (Hata et al., 1998). Smad6 inhibits Bmp4 signaling by (i) binding to Bmp4 bound receptors and targeting them degradation (Hata et al., 1998), (ii) binding pSmad1 and inhibiting its translocation into the nucleus (Hata et al., 1998) and (iii) binding pSmad1 and facilitating Smurf-mediated ubiquitination and subsequent proteosomal degradation of pSmad1 (Murakami et al., 2003; Zhang et al., 2001). We assume, for simplicity, that primary inhibitory effect of Smad6 on pSmad1 is the Smurf-mediated degradation of pSmad1. Runx1 can participate in Bmp4 signaling by binding to pSmad1 in the nucleus and affecting its transcription factor activity (Zaidi et al., 2002). Moreover Smad6 can bind to Runx1 and target it to the proteasome similar to its effect on pSmad1 (Shen et al., 2006). We include the following post-translational reactions in our model to reflect a simplified version of the Bmp4 signaling pathway and Runx1's interaction with Smads.

- Bmp4 binds to a cell-surface receptor leading to the phosphorylation of the regulatory Smad Smad1 (Larsson and Karlsson, 2005; Paulsen et al., 2011). We model the phosphorylation of Smad1 as a simple first-order reaction and use the rate of phosphorylation, k_p, as a proxy for the Bmp4 dose.

$$\mathrm{Smad\ 1}\overset{k_p}{\Longrightarrow}\mathrm{pSmad\ 1} \tag{10}$$

- Smad1 localization in the nucleus has been shown to be Runx1 dependent (Zaidi et al., 2002). In our model, we assume that Runx1 binds, reversibly, to phosphorylated Smad1 (pSmad1) and that this complex can affect transcriptional regulation (Zaidi et al., 2002).

$$\mathrm{pSmad1}\ +\ \mathrm{Runx1}\underset{k_{d1}}{\overset{k_{b1}}{\rightleftharpoons}}\mathrm{pSmad1{-}Runx1} \tag{11}$$

- Smad6 binds to pSmad1 and Runx1 to form complexes that are targeted for Smurf-mediated proteolytic degradation (Hata et al., 1998; Murakami et al., 2003; Zhang et al., 2001). Proteolytic degradation is modeled as a first-order reaction.

$$\mathrm{pSmad1}+\ \mathrm{Smad6}\ \underset{k_d}{\overset{k_b}{\rightleftharpoons}}\mathrm{pSmad1{-}Smad6}\overset{k_{prot}}{\Longrightarrow}\varnothing \tag{12}$$

$$\mathrm{Runx1}+\ \mathrm{Smad6}\ \underset{k_d}{\overset{k_b}{\rightleftharpoons}}\mathrm{Runx1{-}mad6}\overset{k_{prot}}{\Longrightarrow}\varnothing \tag{13}$$

- We also include a partner-switching reaction in which Smad6 replaces Runx1 in the pSmad1–Runx1 complex. The resulting pSmad1–Smad6 is targeted for proteolytic degradation as above.

$$\mathrm{pSmad1{-}Runx1}+\ \mathrm{Smad6}\overset{k_b}{\Longrightarrow}\mathrm{pSmad1{-}Smad6}+\ \mathrm{Runx1} \tag{14}$$

$$\mathrm{pSmad1{-}Smad6}\overset{k_{prot}}{\Longrightarrow}\varnothing \tag{15}$$

The parameter values for all post-translational reactions are given in Table S6. To model the effect of proteosomal inhibition by Bortezomib (BTZ) the proteolytic degradation rate, k_{prot}, was set to zero.

Model equations

All model details are used to derive the following system of ODEs that describe the GRN under consideration:

$$\begin{aligned}
\frac{d[S]}{dt} &= v_s - k^S_{deg}[S]\\
\frac{d[G]}{dt} &= v_g - k^G_{deg}[G]\\
\frac{d[F]}{dt} &= v_f - k^F_{deg}[F]\\
\frac{d[S1]}{dt} &= v_{s1} - k_p[S1] - k^{S1}_{deg}[S1]\\
\frac{d[pS1]}{dt} &= k_p[S1] - [pS1](k_b[S6]+k_{b1}[R]) + k_d[pS1{-}S6]\\
&\quad + k_{d1}[pS1{-}R] - k^{S1}_{deg}[pS1]\\
\frac{d[S6]}{dt} &= v_{s6} - k_b[S6]([pS1]+[R]+[pS1{-}R]) + k_d([pS1{-}S6]\\
&\quad + [R{-}S6]) - k^{S6}_{deg}[S6]\\
\frac{d[R]}{dt} &= v_{rr} + v_r - [R](k_b[S6]+k_{b1}[pS1]) + k_d[R{-}S6] + k_{d1}[pS1{-}R]\\
&\quad + k_b[pS1{-}R][S6] - k^R_{deg}[R]\\
\frac{d[pS1{-}S6]}{dt} &= k_b[S6]([pS1]+[pS1{-}R]) - k_d[pS1{-}S6] - k_{\mathrm{prot}}[pS1{-}S6]\\
&\quad - k^{S1}_{deg}[pS1{-}S6]\\
\frac{d[R{-}S6]}{dt} &= k_b[R][S6] - k_d[R{-}S6] - k_{\mathrm{prot}}[R{-}S6] - k^R_{deg}[R{-}S6]
\end{aligned}$$

$$\frac{d[\mathrm{pS1}{-}R]}{dt} = k_{b1}[R][\mathrm{pS1}]{-}k_{d1}[\mathrm{pS1}{-}R]{-}k_b[\mathrm{pS1}{-}R][\mathrm{S6}]{-}k_{deg}^{S1}[\mathrm{pS1}{-}R] \quad (16)$$

here v_{rr} in the differential equation for [R] is included to model Runx1 overexpression (see Fig. 4). v_{rr} was set to 100 h^{-1} for Fig. 4B.

ODEs for all models (WT and mutants) were solved using the command-line bifurcation package CL-MATCONT (Dhooge et al., 2003) to obtain the steady-state signal–response curves (one-parameter bifurcation diagrams) containing range of signals for which two different steady states are possible. The package was also used to obtain the two-parameter bifurcation diagrams which depict the range of parameter values for which two different steady states are possible. For all models, dynamics to step-input in the Bmp4 signal were analyzed using the *ode23s* solver in MATLAB 2010a(R) (MathWorks, Natick, Massachusetts). Dimensionless models were used in all simulations.

Acknowledgements

This work is partially supported by a John Dunn Foundation award to OAI, HHMI International Student Research Fellowship to JN, National Health and Medical Research Council of Australia project grants to JEP and OAI, and Australian Postgraduate and Translational Cancer Research Network awards to JMB. CJW was supported by REU supplement to NSF CAREER Grant MCB-0845919 to OAI.

Appendix A. Supporting information

Supplementary data associated with this article can be found in the online version at http://dx.doi.org/10.1016/j.ydbio.2013.04.016.

References

Attisano, L., Wrana, J.L., 2002. Signal transduction by the TGF-beta superfamily. Science 296, 1646–1647.
Bee, T., Ashley, E.L., Bickley, S.R., Jarratt, A., Li, P.S., Sloane-Stanley, J., Gottgens, B., de Bruijn, M.F., 2009a. The mouse Runx1 +23 hematopoietic stem cell enhancer confers hematopoietic specificity to both Runx1 promoters. Blood 113, 5121–5124.
Bee, T., Liddiard, K., Swiers, G., Bickley, S.R., Vink, C.S., Jarratt, A., Hughes, J.R., Medvinsky, A., de Bruijn, M.F., 2009b. Alternative Runx1 promoter usage in mouse developmental hematopoiesis. Blood Cells Mol. Dis. 43, 35–42.
Bertrand, J.Y., Chi, N.C., Santoso, B., Teng, S., Stainier, D.Y., Traver, D., 2010. Haematopoietic stem cells derive directly from aortic endothelium during development. Nature 464, 108–111.
Bintu, L., Buchler, N.E., Garcia, H.G., Gerland, U., Hwa, T., Kondev, J., Phillips, R., 2005. Transcriptional regulation by the numbers: models. Curr. Opin. Genet. Dev. 15, 116–124.
Boisset, J.C., van Cappellen, W., Andrieu-Soler, C., Galjart, N., Dzierzak, E., Robin, C., 2010. In vivo imaging of haematopoietic cells emerging from the mouse aortic endothelium. Nature 464, 116–120.
Cai, Z., de Bruijn, M., Ma, X., Dortland, B., Luteijn, T., Downing, R.J., Dzierzak, E., 2000. Haploinsufficiency of AML1 affects the temporal and spatial generation of hematopoietic stem cells in the mouse embryo. Immunity 13, 423–431.
Chen, M.J., Yokomizo, T., Zeigler, B.M., Dzierzak, E., Speck, N.A., 2009. Runx1 is required for the endothelial to haematopoietic cell transition but not thereafter. Nature 457, 887–891.
Davidson, E.H., 2006. The Regulatory Genome: Gene Regulatory Networks in Development and Evolution. Elsevier/Academic Press, Amsterdam; Boston.
Dhooge, A., Govaerts, W., Kuznetsov, Y.A., 2003. MATCONT: a MATLAB package for numerical bifurcation analysis of ODEs. ACM Trans. Math. Software 29, 141–164.
Durand, C., Robin, C., Bollerot, K., Baron, M..H., Ottersbach, K., Dzierzak, E., 2007. Embryonic stromal clones reveal developmental regulators of definitive hematopoietic stem cells. Proc. Nat. Acad. Sci. U.S.A. 104, 20838–20843.
Eilken, H.M., Nishikawa, S., Schroeder, T., 2009. Continuous single-cell imaging of blood generation from haemogenic endothelium. Nature 457, 896–900.
Fontich, E., Sardanyes, J., 2008. General scaling law in the saddle-node bifurcation: a complex phase space study. J. Phys. A: Math. Theor., 41.
Gottgens, B., Nastos, A., Kinston, S., Piltz, S., Delabesse, E.C., Stanley, M., Sanchez, M.. J., Ciau-Uitz, A., Patient, R., Green, A.R., 2002. Establishing the transcriptional programme for blood: the SCL stem cell enhancer is regulated by a multiprotein complex containing Ets and GATA factors. EMBO J. 21, 3039–3050.
Guiu, J., Shimizu, R., D'Altri, T., Fraser, S.T., Hatakeyama, J., Bresnick, E.H., Kageyama, R., Dzierzak, E., Yamamoto, M., Espinosa, L., Bigas, A., 2013. Hes repressors are essential regulators of hematopoietic stem cell development downstream of Notch signaling. J. Exp. Med. 210, 71–84.
Hadland, B.K., Huppert, S.S., Kanungo, J., Xue, Y., Jiang, R., Gridley, T., Conlon, R..A., Cheng, A.M., Kopan, R., Longmore, G.D., 2004. A requirement for Notch1 distinguishes 2 phases of definitive hematopoiesis during development. Blood 104, 3097–3105.
Hart, A., Melet, F., Grossfeld, P., Chien, K., Jones, C., Tunnacliffe, A., Favier, R., Bernstein, A., 2000. Fli-1 is required for murine vascular and megakaryocytic development and is hemizygously deleted in patients with thrombocytopenia. Immunity 13, 167–177.
Hata, A., Lagna, G., Massague, J., Hemmati-Brivanlou, A., 1998. Smad6 inhibits BMP/Smad1 signaling by specifically competing with the Smad4 tumor suppressor. Genes Dev. 12, 186–197.
Ishida, W., Hamamoto, T., Kusanagi, K., Yagi, K., Kawabata, M., Takehara, K., Sampath, T.K., Kato, M., Miyazono, K., 2000. Smad6 is a Smad1/5-induced smad inhibitor. Characterization of bone morphogenetic protein-responsive element in the mouse Smad6 promoter. J. Biol. Chem. 275, 6075–6079.
Kaimakis, P., Crisan, M., Dzierzak, E., 2013. The biochemistry of hematopoietic stem cell development. Biochim. Biophys. Acta 1830, 2395–2403.
Kataoka, H., Hayashi, M., Nakagawa, R., Tanaka, Y., Izumi, N., Nishikawa, S., Jakt, M.L., Tarui, H., 2011. Etv2/ER71 induces vascular mesoderm from Flk1+PDGFRalpha+ primitive mesoderm. Blood 118, 6975–6986.
Knezevic, K., Bee, T., Wilson, N.K., Janes, M..E., Kinston, S., Polderdijk, S., Kolb-Kokocinski, A., Ottersbach, K., Pencovich, N., Groner, Y., de Bruijn, M., Gottgens, B., Pimanda, J.E., 2011. A Runx1-Smad6 rheostat controls Runx1 activity during embryonic hematopoiesis. Mol. Cell Biol. 31, 2817–2826.
Kretzschmar, M., Liu, F., Hata, A., Doody, J., Massague, J., 1997. The TGF-beta family mediator Smad1 is phosphorylated directly and activated functionally by the BMP receptor kinase. Genes Dev. 11, 984–995.
Kumano, K., Chiba, S., Kunisato, A., Sata, M., Saito, T., Nakagami-Yamaguchi, E., Yamaguchi, T., Masuda, S., Shimizu, K., Takahashi, T., Ogawa, S., Hamada, Y., Hirai, H., 2003. Notch1 but not Notch2 is essential for generating hematopoietic stem cells from endothelial cells. Immunity 18, 699–711.
Lacaud, G., Gore, L., Kennedy, M., Kouskoff, V., Kingsley, P., Hogan, C., Carlsson, L., Speck, N., Palis, J., Keller, G., 2002. Runx1 is essential for hematopoietic commitment at the hemangioblast stage of development in vitro. Blood 100, 458–466.
Lacaud, G., Kouskoff, V., Trumble, A., Schwantz, S., Keller, G., 2004. Haploinsufficiency of Runx1 results in the acceleration of mesodermal development and hemangioblast specification upon in vitro differentiation of ES cells. Blood 103, 886–889.
Lancrin, C., Sroczynska, P., Stephenson, C., Allen, T., Kouskoff, V., Lacaud, G., 2009. The haemangioblast generates haematopoietic cells through a haemogenic endothelium stage. Nature 457, 892–895.
Larsson, J., Karlsson, S., 2005. The role of Smad signaling in hematopoiesis. Oncogene 24, 5676–5692.
Li, Z., Chen, M.J., Stacy, T., Speck, N.A., 2006. Runx1 function in hematopoiesis is required in cells that express Tek. Blood 107, 106–110.
Li, Z., Lan, Y., He, W., Chen, D., Wang, J., Zhou, F., Wang, Y., Sun, H., Chen, X., Xu, C., Li, S., Pang, Y., Zhang, G., Yang, L., Zhu, L., Fan, M., Shang, A., Ju, Z., Luo, L., Ding, Y., Guo, W., Yuan, W., Yang, X., Liu, B., 2012. Mouse embryonic head as a site for hematopoietic stem cell development. Cell Stem Cell 11, 663–675.
Liakhovitskaia, A., Gribi, R., Stamateris, E., Villain, G., Jaffredo, T., Wilkie, R., Gilchrist, D., Yang, J., Ure, J., Medvinsky, A., 2009. Restoration of Runx1 expression in the Tie2 cell compartment rescues definitive hematopoietic stem cells and extends life of Runx1 knockout animals until birth. Stem Cells 27, 1616–1624.
Ling, K.W., Ottersbach, K., van Hamburg, J.P., Oziemlak, A., Tsai, F.Y., Orkin, S.H., Ploemacher, R., Hendriks, R.W., Dzierzak, E., 2004. GATA-2 plays two functionally distinct roles during the ontogeny of hematopoietic stem cells. J. Exp. Med. 200, 871–882.
Lugus, J.J., Chung, Y.S., Mills, J.C., Kim, S.I., Grass, J., Kyba, M., Doherty, J.M., Bresnick, E.H., Choi, K., 2007. GATA2 functions at multiple steps in hemangioblast development and differentiation. Development 134, 393–405.
Lux, C.T., Yoshimoto, M., McGrath, K., Conway, S.J., Palis, J., Yoder, M.C., 2008. All primitive and definitive hematopoietic progenitor cells emerging before E10 in the mouse embryo are products of the yolk sac. Blood 111, 3435–3438.
Marks-Bluth, J., Pimanda, J.E., 2012. Cell signalling pathways that mediate haematopoietic stem cell specification. Int. J. Biochem. Cell Biol..
Medvinsky, A., Dzierzak, E., 1996. Definitive hematopoiesis is autonomously initiated by the AGM region. Cell 86, 897–906.
Medvinsky, A., Rybtsov, S., Taoudi, S., 2011. Embryonic origin of the adult hematopoietic system: advances and questions. Development 138, 1017–1031.
Mirny, L.A., 2010. Nucleosome-mediated cooperativity between transcription factors. Proc. Nat. Acad. Sci. U.S.A. 107, 22534–22539.
Mukherjee, S., Raje, N., Schoonmaker, J.A., Liu, J.C., Hideshima, T., Wein, M.N., Jones, D.C., Vallet, S., Bouxsein, M.L., Pozzi, S., Chhetri, S., Seo, Y.D., Aronson, J.P., Patel, C., Fulciniti, M., Purton, L.E., Glimcher, L.H., Lian, J.B., Stein, G., Anderson, K.C., Scadden, D.T., 2008. Pharmacologic targeting of a stem/progenitor population in vivo is associated with enhanced bone regeneration in mice. J. Clin Invest. 118, 491–504.
Murakami, G., Watabe, T., Takaoka, K., Miyazono, K., Imamura, T., 2003. Cooperative inhibition of bone morphogenetic protein signaling by Smurf1 and inhibitory Smads. Mol. Biol. Cell 14, 2809–2817.

Nakagawa, M., Ichikawa, M., Kumano, K., Goyama, S., Kawazu, M., Asai, T., Ogawa, S., Kurokawa, M., Chiba, S., 2006. AML1/Runx1 rescues Notch1-null mutation-induced deficiency of para-aortic splanchnopleural hematopoiesis. Blood 108, 3329–3334.

Narula, J., Igoshin, O.A., 2010. Thermodynamic models of combinatorial gene regulation by distant enhancers. IET Syst. Biol. 4 393–U166.

Narula, J., Smith, A.M., Gottgens, B., Igoshin, O.A., 2010. Modeling reveals bistability and low-pass filtering in the network module determining blood stem cell fate. PLoS Comput. Biol. 6, e1000771.

Nottingham, W.T., Jarratt, A., Burgess, M., Speck, C.L., Cheng, J.F., Prabhakar, S., Rubin, E.M., Li, P.S., Sloane-Stanley, J., Kong, A.S.J., de Bruijn, M.F., 2007. Runx1-mediated hematopoietic stem-cell emergence is controlled by a Gata/Ets/SCL-regulated enhancer. Blood, 110; 4188–4197.

Oren, T., Torregroza, I., Evans, T., 2005. An Oct-1 binding site mediates activation of the gata2 promoter by BMP signaling. Nucleic Acids Res. 33, 4357–4367.

Orkin, S.H., Zon, L.I., 2008. Hematopoiesis: an evolving paradigm for stem cell biology. Cell 132, 631–644.

Paulsen, M., Legewie, S., Eils, R., Karaulanov, E., Niehrs, C., 2011. Negative feedback in the bone morphogenetic protein 4 (BMP4) synexpression group governs its dynamic signaling range and canalizes development. Proc. Nat. Acad. Sci. U.S.A. 108, 10202–10207.

Pimanda, J.E., Donaldson, I.J., de Bruijn, M.F., Kinston, S., Knezevic, K., Huckle, L., Piltz, S., Landry, J.R., Green, A.R., Tannahill, D., Gottgens, B., 2007a. The SCL transcriptional network and BMP signaling pathway interact to regulate RUNX1 activity. Proc. Nat. Acad. Sci. U.S.A. 104, 840–845.

Pimanda, J.E., Gottgens, B., 2010. Gene regulatory networks governing haematopoietic stem cell development and identity. Int. J. Dev. Biol. 54, 1201–1211.

Pimanda, J.E., Ottersbach, K., Knezevic, K., Kinston, S., Chan, W.Y., Wilson, N.K., Landry, J.R., Wood, A.D., Kolb-Kokocinski, A., Green, A.R., Tannahill, D., Lacaud, G., Kouskoff, V., Gottgens, B., 2007b. Gata2, Fli1, and Scl form a recursively wired gene-regulatory circuit during early hematopoietic development. Proc. Nat. Acad. Sci. U.S.A. 104, 17692–17697.

Rhodes, K.E., Gekas, C., Wang, Y., Lux, C.T., Francis, C.S., Chan, D.N., Conway, S., Orkin, S.H., Yoder, M.C., Mikkola, H.K., 2008. The emergence of hematopoietic stem cells is initiated in the placental vasculature in the absence of circulation. Cell Stem Cell 2, 252–263.

Richard, C., Drevon, C., Canto, P.Y., Villain, G., Bollerot, K., Lempereur, A., Teillet, M. A., Vincent, C., Rossello Castillo, C., Torres, M., Piwarzyk, E., Speck, N.A., Souyri, M., Jaffredo, T., 2013. Endothelio–mesenchymal interaction controls runx1 expression and modulates the notch pathway to initiate aortic hematopoiesis. Dev. Cell. 24, 600–611.

Robb, L., Lyons, I., Li, R., Hartley, L., Kontgen, F., Harvey, R.P., Metcalf, D., Begley, C.G., 1995. Absence of yolk sac hematopoiesis from mice with a targeted disruption of the scl gene. Proc. Nat. Acad. Sci. U.S.A. 92, 7075–7079.

Robert-Moreno, A., Espinosa, L., de la Pompa, J.L., Bigas, A., 2005. RBPjkappa-dependent Notch function regulates Gata2 and is essential for the formation of intra-embryonic hematopoietic cells. Development 132, 1117–1126.

Schlaeger, T.M., Mikkola, H.K., Gekas, C., Helgadottir, H.B., Orkin, S.H., 2005. Tie2Cre-mediated gene ablation defines the stem-cell leukemia gene (SCL/tal1)-dependent window during hematopoietic stem-cell development. Blood 105, 3871–3874.

Sciammas, R., Li, Y., Warmflash, A., Song, Y., Dinner, A.R., Singh, H., 2011. An incoherent regulatory network architecture that orchestrates B cell diversification in response to antigen signaling. Mol. Syst. Biol. 7, 495.

Shen, R., Chen, M., Wang, Y.J., Kaneki, H., Xing, L., O'Keefe, R.J., Chen, D., 2006. Smad6 interacts with Runx2 and mediates Smad ubiquitin regulatory factor 1-induced Runx2 degradation. J. Biol. Chem. 281, 3569–3576.

Shivdasani, R.A., Mayer, E.L., Orkin, S.H., 1995. Absence of blood formation in mice lacking the T-cell leukaemia oncoprotein tal-1/SCL. Nature 373, 432–434.

Singbrant, S., Karlsson, G., Ehinger, M., Olsson, K., Jaako, P., Miharada, K., Stadtfeld, M., Graf, T., Karlsson, S., 2010. Canonical BMP signaling is dispensable for hematopoietic stem cell function in both adult and fetal liver hematopoiesis, but essential to preserve colon architecture. Blood 115, 4689–4698.

Smith, A.M., Sanchez, M.J., Follows, G.A., Kinston, S., Donaldson, I.J., Green, A.R., Gottgens, B., 2008. A novel mode of enhancer evolution: the Tal1 stem cell enhancer recruited a MIR element to specifically boost its activity. Genome Res. 18, 1422–1432.

Tanaka, Y., Hayashi, M., Kubota, Y., Nagai, H., Sheng, G., Nishikawa, S., Samokhvalov, I.M., 2012. Early ontogenic origin of the hematopoietic stem cell lineage. Proc. Nat. Acad. Sci. U.S.A. 109, 4515–4520.

Tiwari, A., Balazsi, G., Gennaro, M.L., Igoshin, O.A., 2010. The interplay of multiple feedback loops with post-translational kinetics results in bistability of mycobacterial stress response. Phys. Biol. 7, 036005.

Tiwari, A., Igoshin, O.A., 2012. Coupling between feedback loops in autoregulatory networks affects bistability range, open-loop gain and switching times. Phys. Biol. 9, 055003.

Tsai, F.Y., Keller, G., Kuo, F.C., Weiss, M., Chen, J., Rosenblatt, M., Alt, F.W., Orkin, S.H., 1994. An early haematopoietic defect in mice lacking the transcription factor GATA-2. Nature 371, 221–226.

Wareing, S., Eliades, A., Lacaud, G., Kouskoff, V., 2012. ETV2 expression marks blood and endothelium precursors, including hemogenic endothelium, at the onset of blood development. Dev. Dyn. 241, 1454–1464.

Yen, H.C., Xu, Q., Chou, D.M., Zhao, Z., Elledge, S.J., 2008. Global protein stability profiling in mammalian cells. Science 322, 918–923.

Zafonte, B.T., Liu, S., Lynch-Kattman, M., Torregroza, I., Benvenuto, L., Kennedy, M., Keller, G., Evans, T., 2007. Smad1 expands the hemangioblast population within a limited developmental window. Blood 109, 516–523.

Zaidi, S.K., Sullivan, A.J., van Wijnen, A.J., Stein, J.L., Stein, G.S., Lian, J.B., 2002. Integration of Runx and Smad regulatory signals at transcriptionally active subnuclear sites. Proc. Nat. Acad. Sci. U.S.A. 99, 8048–8053.

Zhang, Y., Chang, C., Gehling, D.J., Hemmati-Brivanlou, A., Derynck, R., 2001. Regulation of Smad degradation and activity by Smurf2, an E3 ubiquitin ligase. Proc. Nat. Acad. Sci. U.S.A. 98, 974–979.

Zovein, A.C., Hofmann, J.J., Lynch, M., French, W.J., Turlo, K.A., Yang, Y., Becker, M.S., Zanetta, L., Dejana, E., Gasson, J.C., Tallquist, M.D., Iruela-Arispe, M.L., 2008. Fate tracing reveals the endothelial origin of hematopoietic stem cells. Cell Stem Cell 3, 625–636.